Developmental Biology 405 (2015) 21–32

Contents lists available at ScienceDirect

Developmental Biology

journal homepage: www.elsevier.com/locate/developmentalbiology

Control of stomach smooth muscle development and intestinal rotation by transcription factor BARX1

Chenura D. Jayewickreme [a], Ramesh A. Shivdasani [a,b,*]

[a] Department of Medical Oncology, Dana-Farber Cancer Institute, 450 Brookline Avenue, Boston, MA 02215, USA
[b] Departments of Medicine, Brigham & Women's Hospital and Harvard Medical School, 450 Brookline Avenue, Boston, MA 02215, USA

ARTICLE INFO

Article history:
Received 15 October 2014
Received in revised form
11 May 2015
Accepted 15 May 2015
Available online 6 June 2015

Keywords:
Digestive tract development
Enteric muscle differentiation
Gut patterning
Homeotic genes

ABSTRACT

Diverse functions of the homeodomain transcription factor BARX1 include Wnt-dependent, non-cell autonomous specification of the stomach epithelium, tracheo-bronchial septation, and Wnt-independent expansion of the spleen primordium. Tight spatio-temporal regulation of *Barx1* levels in the mesentery and stomach mesenchyme suggests additional roles. To determine these functions, we forced constitutive BARX1 expression in the *Bapx1* expression domain, which includes the mesentery and intestinal mesenchyme, and also examined *Barx1*$^{-/-}$ embryos in further detail. Transgenic embryos invariably showed intestinal truncation and malrotation, in part reflecting abnormal left-right patterning. Ectopic BARX1 expression did not affect intestinal epithelium, but intestinal smooth muscle developed with features typical of the stomach wall. BARX1, which is normally restricted to the developing stomach, drives robust smooth muscle expansion in this organ by promoting proliferation of myogenic progenitors at the expense of other sub-epithelial cells. Undifferentiated embryonic stomach and intestinal mesenchyme showed modest differences in mRNA expression and BARX1 was sufficient to induce much of the stomach profile in intestinal cells. However, limited binding at *cis*-regulatory sites implies that BARX1 may act principally through other transcription factors. Genes expressed ectopically in BARX1^{+} intestinal mesenchyme and reduced in *Barx1*$^{-/-}$ stomach mesenchyme include *Isl1*, *Pitx1*, *Six2* and *Pitx2*, transcription factors known to control left-right patterning and influence smooth muscle development. The sum of evidence suggests that potent BARX1 functions in intestinal rotation and stomach myogenesis occur through this small group of intermediary transcription factors.

1. Introduction

Anterior–posterior patterning of the embryonic gut in vertebrate animals produces digestive organs-the esophagus, stomach, and intestines-with characteristic epithelial, sub-epithelial, and mural features. Region-specific interactions between the endoderm-derived epithelium and adjacent mesoderm-derived mesenchyme drive this patterning and depend on transcription factors (TFs) that are expressed in restricted domains (Spence et al., 2011). Among such TFs, expression of the homeodomain protein BARX1 is limited to the esophageal and stomach mesenchyme and required for proper development of both organs (Kim et al., 2005; 2007; Woo et al., 2011). In *ex vivo* cultures, loss of BARX1 from fetal mouse stomach mesenchyme has a non-cell autonomous effect on overlying endoderm, inducing epithelium with intestinal instead of stomach markers (Kim et al., 2005). *Barx1*$^{-/-}$ mouse embryos have a small, dysmorphic foregut with a trachea-esophageal fistula (Woo et al., 2011) and a stomach epithelium replaced by villous, intestine-type mucosa (Kim et al., 2005; 2007). Both these anomalies reflect unchecked Wnt signaling owing to reduced mesenchymal production of the Wnt antagonists SFRP1 and SFRP2 (Kim et al., 2005; Woo et al., 2011). *Barx1* is also expressed in the spleen anlage, which arises adjacent to the stomach, and although the *Barx1*$^{-/-}$ spleen is miniscule, this defect is unrelated to SFRPs or Wnt signaling (Kim et al., 2007). Thus, BARX1 helps pattern the mammalian foregut, in part through local inhibition of Wnt signaling, and has Wnt-independent requirements in spleen development.

Other important aspects of *Barx1* function and mechanisms remain unknown: Does the non-cell autonomous effect on overlying gut endoderm force stomach differentiation or merely avoid the intestinal fate? Is induction of stomach-type epithelium its predominant function or does BARX1 have additional, cell-autonomous requirements in foregut mesenchyme? In addition to the stomach wall, *Barx1* is expressed in portions of the mesentery, the loose mesoderm-derived membrane that attaches bowel loops to each other and to the dorsal body wall. *Barx1*'s role in spleen

* Corresponding author at: Dana-Farber Cancer Institute, 450 Brookline Avenue, Boston, MA 02215, USA.
E-mail address: ramesh_shivdasani@dfci.harvard.edu (R.A. Shivdasani).

http://dx.doi.org/10.1016/j.ydbio.2015.05.024
0012-1606/

development seems related to this mesenteric expression (Kim et al., 2007) but its precise expression domain and additional functions are not known.

To address these questions, we forced BARX1 expression in mouse intestinal mesenchyme and the mesentery at levels similar to those present in the native fetal stomach. Ectopic BARX1 expression did not perturb the stomach–intestine boundary or epithelial differentiation, but produced profound cell-autonomous defects in enteric myogenesis and gut rotation. We find that in embryonic gut mesenchyme, BARX1 promotes proliferation of muscle cell progenitors at the expense of non-muscle cells; in the mesentery, it controls the gut rotation that is necessary to reverse the physiologic umbilical hernia. To determine the basis for these developmental functions, we identified embryonic genes that respond to BARX1 in the intestine and depend on BARX1 for expression in the stomach. Our studies suggest that both functions occur through a select group of intermediary transcription factors (TFs), including Pitx2 and Isl1, TFs previously implicated in organ laterality and muscle differentiation. Data from BARX1-overexpressing and *Barx1*$^{-/-}$ embryos corroborated these conclusions. Thus, this study identifies new and distinct roles for BARX1 in abdominal organogenesis and patterning, and reveals key TF targets that likely drive organ positioning and tissue differentiation.

2. Materials and methods

Mice. To generate Cre-activated *Barx1*^{Int} mice, we inserted a *LoxP*-flanked *Neo*^{R} stop cassette and *Barx1* cDNA (Fig. 1A) into pROSA26-1 (Zambrowicz et al., 1997), electroporated JM8 ES cells with the resulting targeting construct, and screened ES cell clones by Southern blotting to identify homologous recombinants. We verified correct targeting at the 5' end by PCR (Fig. 1B) using primers complementary to exon 1 of *Rosa26* (CCTAAAGAAGAGGCTGTGCTTTGG) and the *Neo*^{r} cassette (TGAATGAACTGCAGGACGAGGCAG), which yield a 2040-bp product. At the 3' end, primers complementary to *Barx1* (AGCCTCGACTGTGCCTTCTA) and exon 2 of *Rosa26* (TGTTCAAGCAGGACCAAATGTG) yielded a 4775-bp product. Transgenic mice were subsequently genotyped by PCR (Fig. 1B) using a common forward primer in intron 1 of *Rosa26* (GAGTTCTCTGCTGCCTCCTG), with reverse primers in this intron to amplify a 600-bp product G–C from the untargeted allele (GCCAATGCTCTGTCTAGGGG) or 3' to the proximal *LoxP* site to amplify a 320-bp product G–M from the targeted allele (GTTCTTCTGAGGGGATCGGC). *Bapx1-Cre* (Verzi et al., 2009), *Rosa26*^{YFP} (Srinivas et al., 2001), and *Barx1*-null (Kim et al., 2005) mice were described previously. We regarded the morning of a vaginal plug as embryonic day (E) 0.5. Animal care and procedures were approved and monitored by an Institutional Animal Care and Use Committee.

Histology, histochemistry, immunostaining, and microscopy. Whole embryos younger than E14.5 or isolated digestive tracts from older embryos were fixed overnight at 4 °C in 4% paraformaldehyde in phosphate-buffered saline (PBS), washed in PBS, and either frozen in OCT compound (Sakura) to detect YFP expression or dehydrated in ethanol and embedded in paraffin for other analyzes. Ten-μm frozen tissue sections were washed in PBS, stained with DAPI (Vectashield Mounting Media), and examined under a fluorescent microscope or 5- to 6- μm paraffin tissue sections were stained with Hematoxylin and Eosin, Alcian Blue, Periodic Acid Schiff, or Alkaline Phosphatase substrate, or with antibodies (Ab) to BARX1 (Kim et al., 2007) (1:1000), PDX1 (gift of Christopher Wright, Vanderbilt University) (1:1000), SMA-A (Biogenex, 1:300), Ki67 (Thermo Fisher, 1:1000), H/K ATPase (MBL, 1:1000), Pepsinogen (Abcam, 1:1000), or CDX2 (Biogenex, 1:200). Horseradish peroxidase-conjugated secondary Ab (Vector Laboratories) were applied at 1:5000 dilution. Reactions were developed using DAB substrate (Sigma) and slides were counterstained with hematoxylin. The widths of intestinal villi at their base and thickness of circular smooth muscle were measured in transverse tissue sections using ImageJ tools (http://imagej.nih.gov/ij/). Five-μm sections of E17.5 tissues were co-stained on the same slides with SMA-A and Ki67 Ab, followed by FITC- or Cy3-conjugated secondary Ab (Jackson Laboratories, 1:1000). Vectashield mounting media with DAPI (Vector Laboratories) was added prior to imaging at least 6 separate fields in 3 biologic replicates. DAPI+ and Ki67+ nuclei were counted in SMA+ and SMA- sub-epithelium using the Cell Counter plug-in feature in ImageJ (http://imagej.nih.gov/ij/). Histologic comparisons were made between the same regions of the proximal intestine in wild-type and mutant mice. We measured villus width, muscle thickness, and muscle cell fractions in multiple sections of the same regions in control and mutant samples.

Tissue isolation and cell culture. For intestinal and stomach mesenchyme, organs isolated from E13.5 or E17.5 mouse embryos were washed in cold Hank's Buffered Saline Solution (HBSS, Invitrogen) and digested sequentially in 0.1% Collagenase-Dispase (Roche) in HBSS at 37 °C for 30 min and 0.25% Trypsin-EDTA (Invitrogen) at 37 °C for 10 min. Cells were harvested by centrifugation, cultured in Dulbecco's Modified Eagle Medium (Invitrogen) supplemented with glutamine, 20% fetal bovine serum and 1% Penicillin–Streptomycin, and analyzed after a 3-day period in which endodermal derivatives die and highly enriched mesenchyme remains (Kim et al., 2005). E17.5 mesentery was dissected from the whole intestine under microscope guidance and processed immediately for RNA extraction.

Gene expression analyses. Tissues were homogenized in TRIzol reagent (Invitrogen) using a rotor homogenizer, snap frozen, and stored at −80 °C. RNA was isolated with RNeasy mini-kits (QIAGEN), treated with DNaseI, and reverse transcribed using the Superscript III First-Strand Synthesis System (Invitrogen). For quantitative RT-PCR we used FastStart Universal SYBR Green Master Mix (Roche) and gene-specific primers (Suppl. Table 3). Relative mRNA levels were determined using the $\Delta\Delta C_T$ method (Livak and Schmittgen, 2001), with normalization to the levels of *Hprt* mRNA. Graphing and statistical analyzes were performed using GraphPad Prism 6.0 software and *P*-values were calculated using unpaired *t* tests. For transcriptome analyzes, RNA was hybridized to Mouse Genome 430A v2.0 arrays (Affymetrix) and data were analyzed in Gene Pattern (http://genepattern.org) using the Expression File Creator (RMA normalization), Comparative Marker Selection, Principal Component Analysis, and Hierarchical Clustering tools. Data are deposited in the Gene Expression Omnibus (GSE ID: 69483). *Barx1* mRNA in situ hybridization was described previously (Kim et al., 2005).

Chromatin immunoprecipitation (ChIP), sequencing, and analysis. We inserted *Barx1* cDNA with 3 tandem FLAG epitopes immediately after *Egfp* cDNA and P2A cleavage sequences in pUltra and used this construct to produce 3xFlag-Barx1 lentivirus in 293FT cells. This virus was used to infect E13.5 mouse embryonic stomach mesenchymal cells immortalized by expression of a dominant-negative *TRP53* mutant, p53DD (Shaulian et al., 1992). Infected cells were monitored for EGFP expression over 7 days of expansion, then cross-linked with 1.1% formaldehyde in PBS for 10 min at room temperature before nuclei were extracted in a hypotonic buffer (50 mM Tris–HCl, pH 8.0, 85 mM KCl, 0.5% NP-40). Extracts were sonicated (50 mM Tris–HCl, pH 8.1, 10 mM EDTA, 0.1% SDS) to obtain 200- to 500-bp DNA fragments and immunoprecipitated as described previously (Verzi et al., 2010) using 10 μg Flag-M2 Ab (Sigma) and Protein G Dynabeads (Invitrogen). Libraries from the input (sonicated DNA) and ChIP material were prepared using ThruPlex kits (Rubicon Genomics) and sequenced on the Illumina platform. Data are deposited in the

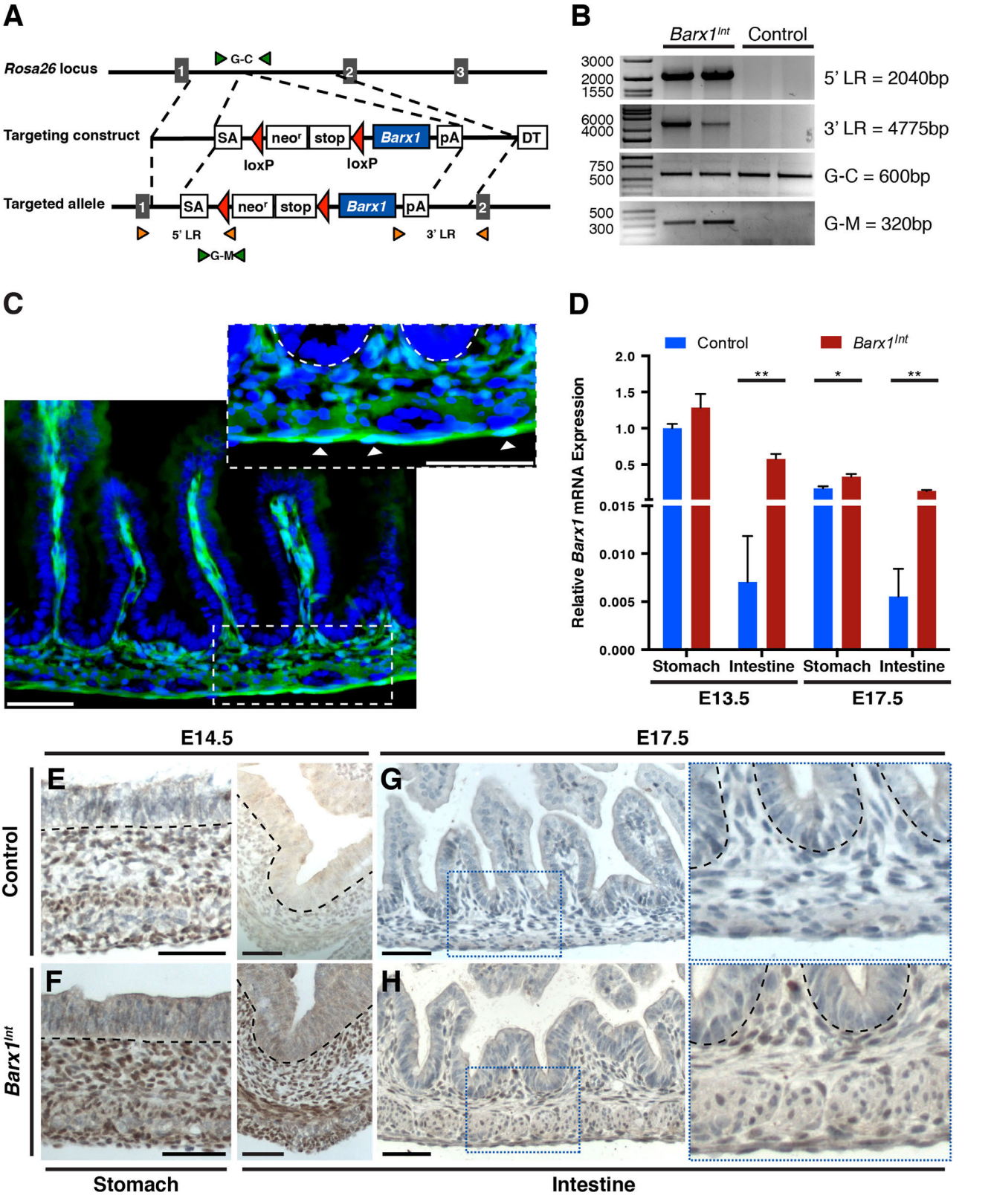

Fig. 1. Strategy and confirmation of ectopic*Barx1*expression. (A) Design of the targeting construct. A *Neo*^{R} Stop cassette flanked by *Lox P* sites and *Barx1* cDNA was introduced between *Rosa26* exons 1 and 2. (B) Long-range PCR was used to confirm homologous recombination at the 5′ and 3′ sides in ES cells and short-range PCR was used to genotype mice, as described in Materials and methods. LR, long-range; G–M, Genotyping-mutant; G–C, Genotyping-control. (C) Fluorescence image of *Bapx1*$^{+/Cre}$;*Rosa26*$^{+/YFP}$ intestines at E17.5, verifying prior Cre activity throughout the muscularis and lamina propria. The inset shows a high-magnification view of the dashed area, with arrowheads pointing to YFP expression in the mesentery. (D) Quantitative RT-PCR analysis of *Barx1* mRNA in isolated control and *Barx1*^{Int} stomachs and intestines at E13.5 and E17.5 ($n=3$ for all samples) revealed significantly increased *Barx1* expression in *Barx1*^{Int} intestines, comparable to levels in wild-type stomach. Bars represent mean ± SEM of biological replicates; $^{*}P<0.05$; $^{**}P<0.005$. (E–H) BARX1 immunohistochemistry (IHC) in *Barx1*^{Int} ($n=3$) and littermate control ($n=4$) stomachs at E14.5 and stomach and intestines at E17.5, confirming ectopic intestinal expression. Blue dotted boxes in G and H indicate areas shown at high magnification to the right. Black dashed lines demarcate borders between the epithelium and mesenchyme. All scale bars, 50 μm.

Gene Expression Omnibus (GSE ID: 69483). BARX1 binding sites were identified using Model-Based Analysis of ChIP-Seq (MACS2) with a q-value cutoff of 0.1 and analyzed using tools in Cistrome (http://cistrome.org/ap/).

3. Results

3.1. Targeted ectopic expression of Barx1 in mouse intestinal mesenchyme and mesentery

We used homologous recombination in embryonic stem (ES) cells to insert inducible *Barx1* cDNA into the *Rosa26* locus. The targeting construct contained a splice-acceptor sequence and a *LoxP*–flanked Neomycin resistance (Neo^R) stop cassette upstream of *Barx1* cDNA (Fig. 1A), to allow Cre-mediated excision of the stop cassette and transgene expression from the targeted $Rosa26^{(L\text{-}S\text{-}L)Barx1}$ allele ($Rosa26^{Bx}$). We activated *Barx1* expression using $Bapx1^{Cre}$ mice, which express Cre recombinase in several abdominal structures, including the mesenchyme of the gastric antrum and of the whole intestine, by E9.5 (Verzi et al., 2009). $Bapx1^{+/Cre}$;$Rosa26^{(L\text{-}S\text{-}L)YFP}$ mouse embryos indicated Cre-activated YFP reporter expression throughout the E13.5 intestinal submucosa, including the lamina propria and smooth muscle (Fig. 1C). Importantly, YFP expression extended to the outermost cell layer, the serosa, which is contiguous with the mesentery (arrowheads in Fig. 1C, inset). We expected $Bapx1^{+/Cre}$;$Rosa26^{+/Bx}$ (henceforth celled $Barx1^{Int}$) mice to express *Barx1* in the same domain, and indeed, mRNA levels in E13.5 $Barx1^{Int}$ intestines were comparable to those in wild-type stomachs and 100 times higher than the levels in wild-type intestines (Fig. 1D). Because Cre-induced deletion of the stop cassette is stably transmitted to all cellular progeny, expression was sustained at E17.5. Immunohistochemistry showed ectopic BARX1 in the intestinal mesenchyme but not in endoderm-derived mucosal cells (Fig. 1E–H). Unlike the stomach, where *Barx1* levels decline significantly after E13.5 (Kim et al., 2005), the protein persisted in E17.5 intestinal mesenchyme, as expected (Fig. 1H).

3.2. Ectopic BARX1 expression produces severe defects in development of the alimentary canal and other abdominal organs

$Barx1^{Int}$ mice died immediately after birth (Fig. 2A). In crosses between $Rosa26^{+/Bx}$ and $Bapx1^{+/Cre}$ parents, however, $Barx1^{Int}$ embryos were present in the correct Mendelian ratios at E13.5 and E17.5, with complete penetrance of defects, such as gastroschisis, which explain neonatal lethality. The physiologic umbilical hernia, which normally reverses by E15, persisted in $Barx1^{Int}$ embryos: a portion of the intestine, including the cecum, invariably lay outside a perforated abdominal wall (Fig. 2B). The small intestine, but not the colon, was markedly reduced in length (Fig. 2C–E). In normal mice, the duodenum first extends away from the stomach before turning 180° (Savin et al., 2011) to encompass the pancreas within the resulting loop (Fig. 2D). In $Barx1^{Int}$ embryos, by contrast, the duodenum was fully apposed to the greater curvature of the stomach, having turned sharply leftward and posteriorly at the pyloric junction (Fig. 2C,D,F), nearly identical to the reported effect of forced symmetry in visceral *Pitx2* expression (Shiratori et al., 2006). In addition, all $Barx1^{Int}$ embryos lacked a spleen (Fig. 2D) and the pancreas was hypoplastic (Fig. 2D) and mispositioned (Fig. 2F–G). A diminutive pancreas was always present in a narrow pocket between the greater curvature of the stomach and the malrotated duodenum (Fig. 2G). Thus, ectopic BARX1 affected the development of abdominal organs profoundly and in a consistent manner.

The mean proportional reduction in small intestine length, measured from pylorus to cecum, was similar at E13.5 at E17.5 (Fig. 2E). Similarly, pancreas defects were evident by E13.5 (Fig. 2F); the gastric antrum, pancreas, and duodenal wall had fused by E14.5 (Fig. 2G); and a spleen was never present. Thus, defects in abdominal organ size and form appeared soon after forced BARX1 expression. In the most overtly affected organ, the intestine, *Barx1* is normally expressed transiently and only in the mesentery (Kim et al., 2005). Therefore, these findings suggest that physiologic attenuation of mesenteric *Barx1* levels is necessary for proper intestinal rotation and length. Notably, absence (Kim et al., 2007) or ectopic expression (Fig. 2D) of BARX1 result in reduced spleen mass and asplenia, respectively, revealing that the spleen anlage is extremely sensitive to the amount or duration of *Barx1* expression.

3.3. Intestinal BARX1 expression preserves epithelial identity

BARX1 expression in embryonic stomach mesenchyme helps specify the overlying gastric epithelium by E13 (Kim et al., 2005; 2007). If this activity represents a dominant, context-independent function, then $Barx1^{Int}$ intestines might show stomach features, especially because they sustain BARX1 expression from an early time. These intestines did not, however, express markers of any gastric lineage: H^+/K^+ ATPase (Atp4b), Pepsinogen, or strong surface affinity for Periodic Acid Schiff (Fig. 3A–C). Other gastric markers were undetectable even by qRT-PCR (Fig. 3D); only *Gastrin*, a hormonal gene normally expressed in stomach and duodenal epithelia, was elevated in $Barx1^{Int}$ intestines (Fig. 3D). CDX2, an intestine-specific transcription factor, was robustly expressed in E12.5 and older $Barx1^{Int}$ intestines (Fig. 3E and F), which showed normal proportions of Alcian blue-avid goblet cells (Fig. 3G) and alkaline phosphatase-expressing enterocytes (Fig. 3H), and normal levels of intervillus cell proliferation (Fig. 3I). Thus, unlike BARX1's potent role in the stomach, it is insufficient to impose stomach differentiation on intestinal endoderm, even with timing and levels of ectopic expression similar to those in the native stomach. In *en face* views of whole-mount intestines, however, some $Barx1^{Int}$ villus profiles appeared abnormally wide (Fig. 3J and K) and close inspection of transverse sections (Suppl. Fig. 1A) supported this observation. Measurements at the villus base confirmed a small but statistically significant increase in average villus width (Fig. 3L). We conclude that *Barx1*'s role in patterning the digestive epithelium is confined to the prospective stomach and that ectopic intestinal expression produces a subtle defect in villus morphology.

3.4. BARX1 induces smooth muscle of a stomach type in the intestine

Stomach smooth muscle is bulky, with thick bundles of alpha-smooth muscle actin (SMA-A) expressing cells in the wall and thick interstitial smooth muscle (muscularis mucosae) present in the lamina propria (Fig. 4A). Normal intestinal muscle has notably less mass and the lamina propria contains a single layer of myofibroblast cells with limited contractility (Powell et al., 2011). These differences in enteric muscles underlie distinct digestive functions – mechanical disruption of food in the stomach and peristaltic propulsion of intestinal luminal contents – but the molecular basis for differential myogenesis is unknown. Unexpectedly, intestinal smooth muscle in $Barx1^{Int}$ mice showed a distinctly gastric character, with thick bundles in the wall and bulky interstitial fibers (Fig. 4A). Smooth muscle was expanded throughout the intestinal length and uniformly around the perimeter (Fig. 4B), with some areas of additional focal hypertrophy (Fig. 4C). Smooth muscle was absent from the pancreas, where minimal SMA-A staining in the parenchyma was similar to that in control

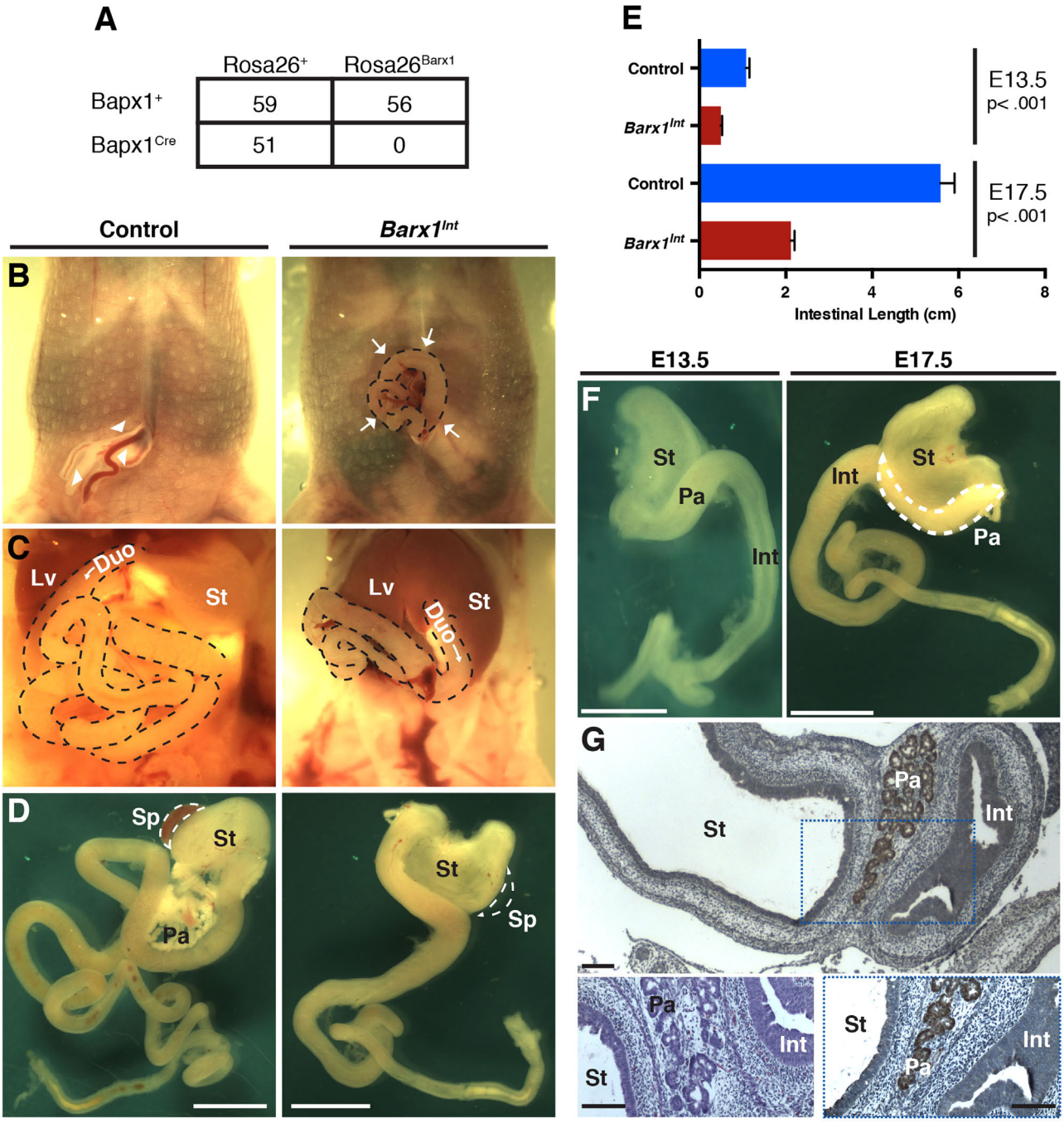

Fig. 2. Intestinal truncation, gut malrotation, asplenia, and pancreas hypoplasia in *Barx1*^{Int} embryos. (A) Crosses between *Rosa26*$^{+/Barx1}$ and *Bapx1*$^{+/Cre}$ parents yielded no live *Barx1*^{Int} pups past birth; other genotypes were represented in Mendelian proportions. (B) E17.5 *Barx1*^{Int} embryos ($n > 50$) showed fully penetrant gastroschisis, with several external intestinal loops (black dashed lines). Arrowheads point to umbilical blood vessels in littermate controls and arrows point to ectopic intestinal loops in *Barx1*^{Int} embryos. (C and D) Abdominal anatomy with the skin removed (C) and the digestive tract isolated (D). *Barx1*^{Int} intestines (dashed black lines) are short and fail to loop away from the stomach; instead, the duodenum attaches to the greater curvature of the stomach (St). The spleen (Sp, dashed white line) is absent and the pancreas (Pa) is severely hypoplastic. (E) Markedly reduced intestinal length, measured from duodenum to cecum in E13.5 and E17.5 *Barx1*^{Int} ($n=8$, $n=7$) and littermate control ($n=9$, $n=10$) embryos. Bars represent the mean ± SEM. (F) Pancreas hypoplasia and mislocalization are apparent in *Barx1*^{Int} embryos at E13.5 and E17.5 ($n > 20$ each). (G) Histologic and IHC confirmation of the pancreas defects, shown with H&E (bottom left) and PDX1 (top) staining. A close-up of the area marked by the dotted blue box is shown at bottom right. Sp, spleen; St, stomach; Pa, pancreas; Int, intestine; Lv, liver. Scale bars: D–F, 2.5 mm; G, 100 μm.

samples and contrasted sharply with strong, uniform staining in the adjoining intestinal wall (Fig. 4D). We detected no hypertrophy of smooth muscle in the gastric pylorus (Suppl. Fig. 1C), where abnormal turning of viscera at the gastro-duodenal junction (Figs. 2D, 2G) precluded strict comparison of the valvular structure with control animals.

We had previously noted patchy musculature in *Barx1*$^{-/-}$ stomachs (Kim et al., 2007), but the significance of this finding in the diminutive mutant organ had been unclear. In light of the smooth muscle abnormalities in *Barx1*^{Int} intestines, we measured expression of myogenic differentiation markers in both settings. Genes with increased mRNA levels in *Barx1*^{Int} intestines showed reduced levels in *Barx1*$^{-/-}$ stomachs, compared to age-matched wild-type littermates, (Fig. 4E). Thus, both gain- and loss-of-function studies support a profound, cell-autonomous effect on enteric smooth muscle development. Smooth muscle, which was

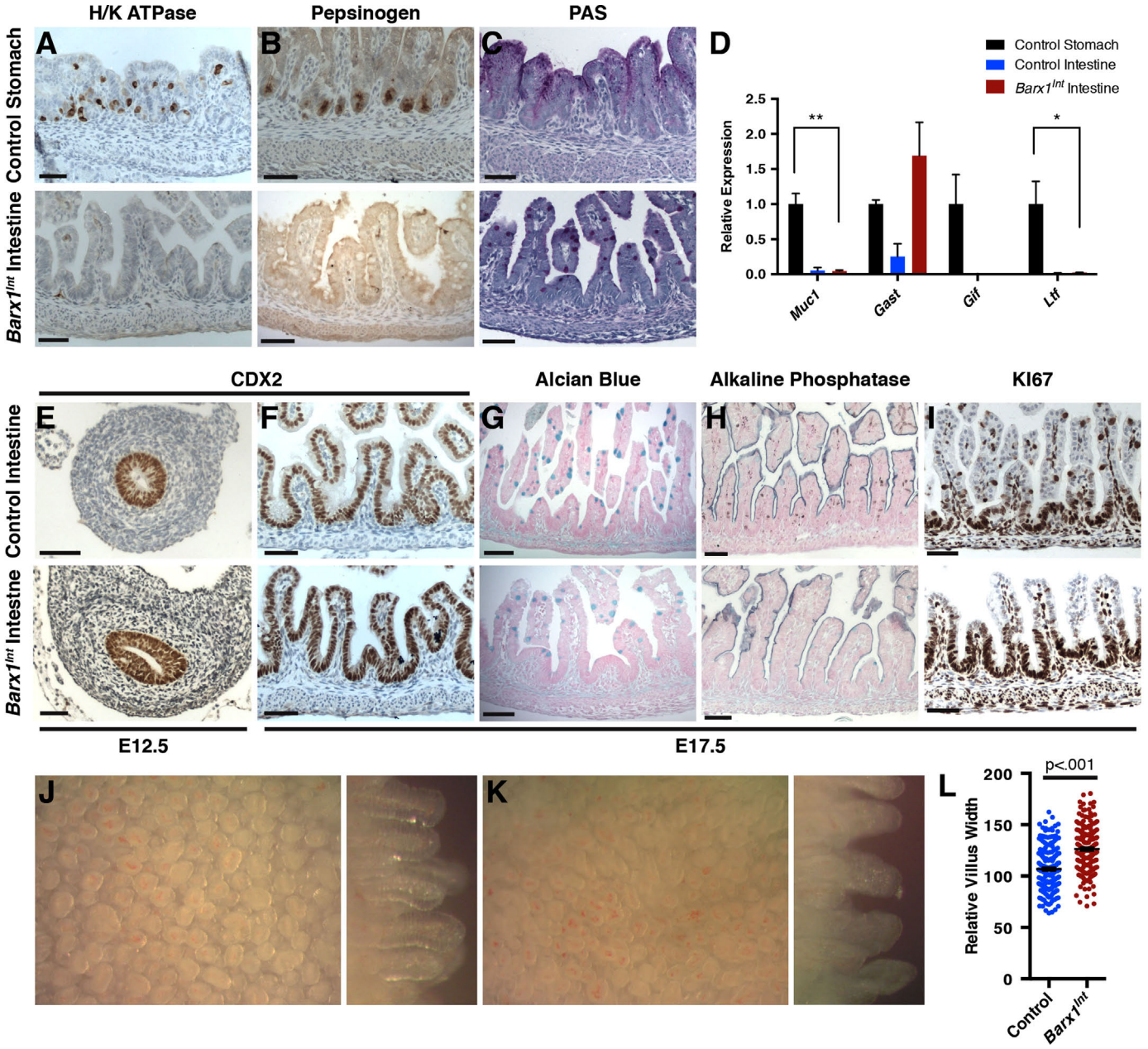

Fig. 3. Intact epithelial differentiation in*Barx1*^{Int} intestines. (A–C) Stomach-specific markers H/K ATPase (A), Pepsinogen (B), and the typical pit-cell pattern of Periodic Acid Schiff (PAS) staining (C) were all readily detected in control stomachs, but not in *Barx1*^{Int} intestines. (D) qRT-PCR analysis showed no increase in expression of stomach-specific genes other than *Gast* in E17.5 *Barx1*^{Int} intestines. Bars represent mean ± SEM of 3 biological replicates for each genotype. (E–H) CDX2 immunohistochemistry (E and F) and goblet cell (G) and enterocyte (H) stains showed the normal patterns of these intestine-specific markers in the same regions of the duodenum in control and *Barx1*^{Int} mice ($n=3$ each). (I) Cell proliferation, as judged by Ki67 immunostaining, was not perturbed in *Barx1*^{Int} intestinal epithelium ($n=3$). (J and K) Whole-mount views of freshly harvested control (J, $n=7$) and *Barx1*^{Int} (K, $n=6$) intestines, showing overtly similar *en face* villus morphology (left images) and modestly wider villi in profile (right images). (L) Small increase in average intestinal villus width in *Barx1*^{Int} intestines, measured in transverse sections of the duodenum ($n=3$ for each genotype). All scale bars, 50 μm.

equally thin in the proximal and distal small intestine in control embryos, was uniformly thickened along the whole small intestine in *Barx1*^{Int} mice and most evident in the inner circular layer and interstitium; the outer layer of longitudinal smooth muscle was too flat to reveal differences from wild-type intestines. Circular smooth muscle thickness was similar to that in wild-type intestines at E14.5 and increased steadily thereafter, with near doubling by E17.5 (Fig. 4F).

This progression (Fig. 4G–I) implies either that muscle progenitors had expanded after mid-gestation or that undifferentiated sub-epithelial mesenchymal cells had adopted the muscle fate. To distinguish between these possibilities, we examined SMA and Ki67 expression (stained with different colors on the same sections) in wild-type stomach and intestine, *Barx1*^{Int} intestines, and *Barx1*$^{-/-}$ stomachs (Fig. 5A–D). We defined muscle cells as SMA^{+} cells with DAPI-stained nuclei; non-muscle cells as sub-epithelial DAPI^{+} cells lacking SMA; and proliferating cells as those expressing Ki67. Compared to wild-type tissues, *Barx1*^{Int} intestines (Fig. 5B,C,E) and *Barx1*$^{-/-}$ stomachs (Fig. 5A,D,E) showed significantly expanded and depleted smooth muscle compartments, respectively. Moreover, *Barx1*^{Int} intestines showed increased proliferation of muscle, and reduced proliferation of non-muscle, cells compared to wild-type littermates (Fig. 5F). By contrast, *Barx1*$^{-/-}$ stomachs showed reduced muscle cell, and increased non-muscle cell, proliferation. Thus, in the enteric wall, BARX1 promotes muscle cell proliferation at the expense of non-muscle cells. In

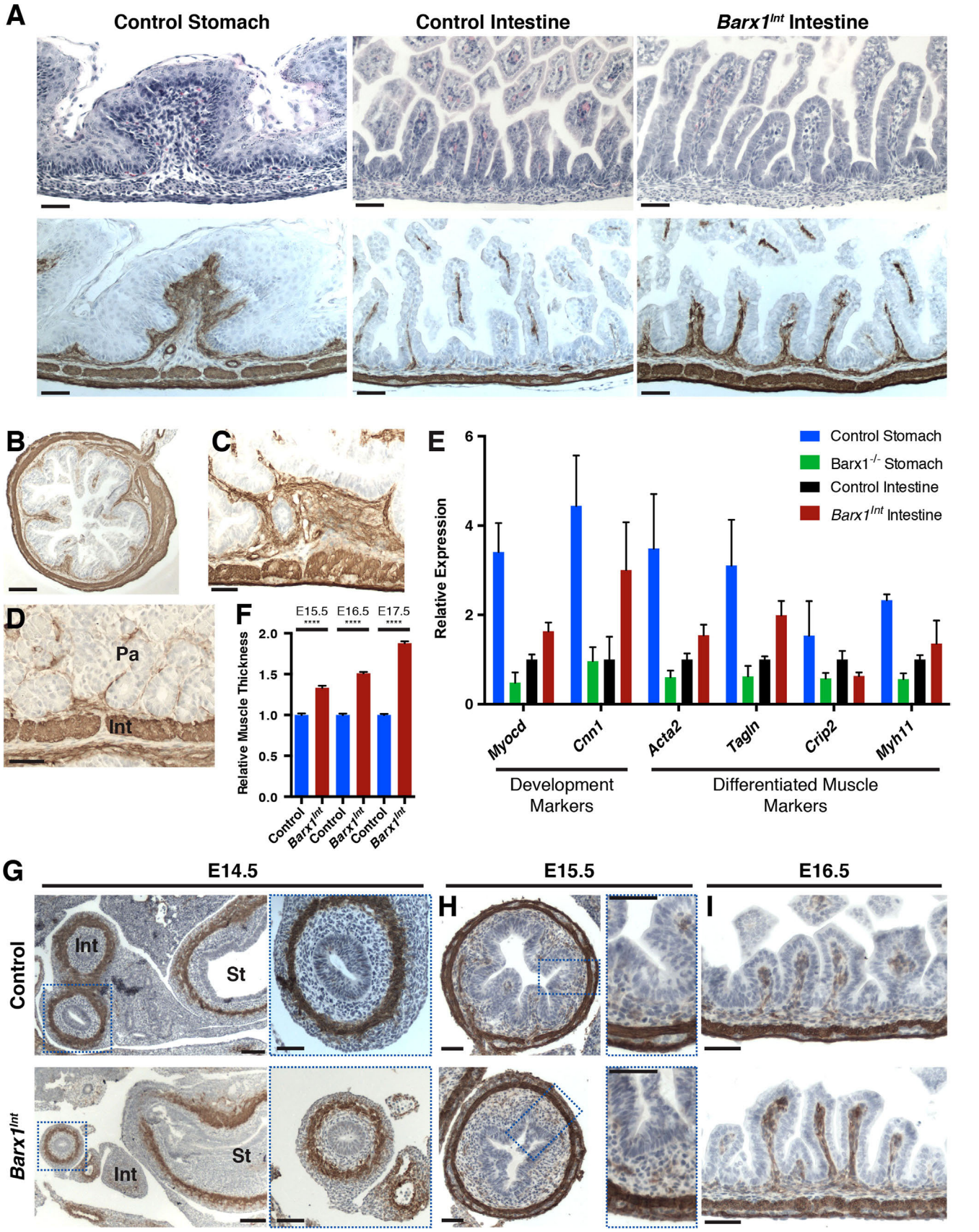

Fig. 4. Smooth muscle expansion in *Barx1*^{Int} intestines. (A) Control (wild-type) stomach and duodenum ($n=3$ each) and *Barx1*^{Int} duodenum ($n=5$) stained with H&E (top) and Alpha-smooth muscle actin (SMA-A) Ab (bottom) reveal significant smooth muscle expansion in the latter. (B–D) SMA-A immunohistochemistry shows this defect in a cross-section of *Barx1*^{Int} intestines (B), areas of dramatic muscle expansion (C), and absence of smooth muscle within the pancreas (D). Pa, pancreas parenchyma; Int, intestinal wall. (E) qRT-PCR analysis of smooth muscle marker genes in whole E17.5 *Barx1*^{Int} and littermate control stomachs and intestines. Bars represent mean ± SEM of biologic replicates, $n=3$ each. (F) Quantitation of circular smooth muscle thickness in 6 transverse sections per sample. The bars represent mean ± SEM of biologic replicates (E15.5 and E16.5, $n=2$ each; E17.5, $n=3$ each). $^{****}P < 0.0001$. (G–I) SMA-A immunostaining shows similar (E14.5) and increased (E15.5 and E16.5) levels of muscle in the same regions of *Barx1*^{Int} and littermate control (E15.5 and E16.5, $n=2$; E14.5, $n=3$) duodenum. St, stomach; Int, intestines. Areas demarcated by dotted blue lines are magnified to the right in G and H. All scale bars, 50 μm.

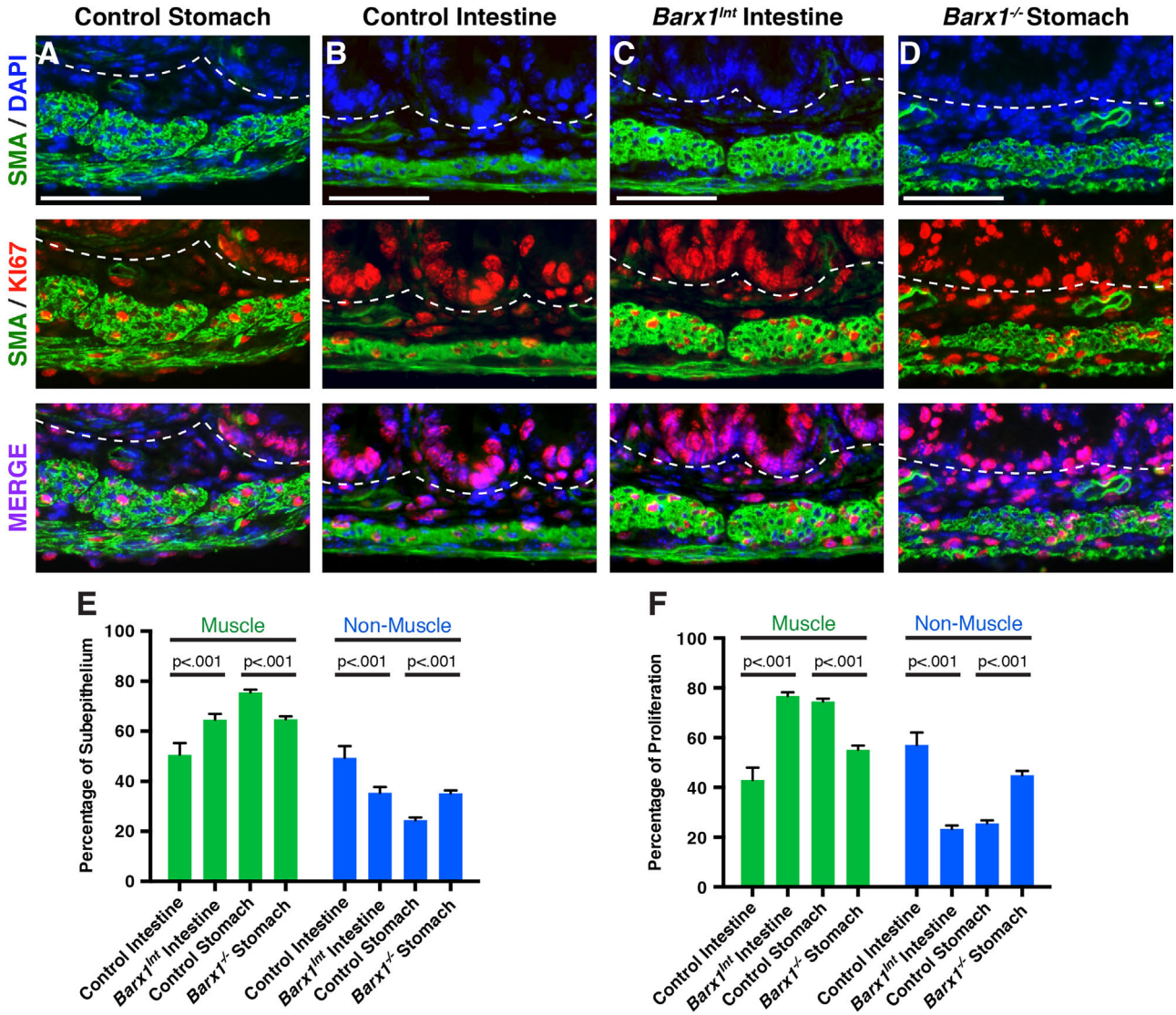

Fig. 5. Increased muscle cell proliferation in *Barx1*^{Int} intestines. (A–D) Fluorescence IHC of E17.5 control and mutant stomachs and intestines (n=3 each) stained simultaneously for SMA-A and DAPI (top), SMA-A and Ki67 (middle), and merged images (bottom). The border between epithelium and mesenchyme is marked with dashed lines. Scale bars, 50 μm. (E) Counts for DAPI^{+} and Ki67^{+} cells in sub-epithelial muscle (SMA^{+}) and non-muscle (SMA^{-}) regions. Six separate areas were analyzed for each indicated tissue sample and genotype (n=3 each). Sub-epithelial composition was determined by comparing the ratio of muscle and non-muscle cells. (F) Fraction of proliferating cells, determined by counting Ki67^{+} cells in muscle and non-muscle compartments. Bars represent mean ± SEM of biologic replicates. Comparisons were made between the same regions of the proximal intestine in wild-type and mutant mice.

contrast to its cell-nonautonomous role in specifying stomach epithelium, this effect in a BARX1-expressing tissue in wild-type and *Barx1*^{Int} mice is likely cell-autonomous.

3.5. *Molecular basis of BARX1-dependent gastric myogenesis and visceral laterality*

The smooth muscle expansion in *Barx1*^{Int} intestines resembles defects observed in *Xenopus* tadpoles with impaired enteric Hedgehog (Hh) signaling (Zhang et al., 2000). Hh signaling also profoundly influences mouse gut myogenesis (Kosinski et al., 2010; Mao et al., 2010; Ramalho-Santos et al., 2000; Zacharias et al., 2011b) and enteric muscle in chick embryos responds to a gradient of endoderm-derived Hh ligands (Sukegawa et al., 2000). Thus, amplified Hh effects on smooth muscle differentiation in the native stomach could potentially explain the excess muscle in *Barx1*^{Int} intestines. However, well-validated markers of Hh signaling were not altered (Suppl. Fig. 1B). These data argue against defective Hh signaling in enteric muscle development and in favor of possible cell-autonomous BARX1 functions.

To identify other potential determinants, we isolated mesenchyme from wild-type stomach and intestine and from *Barx1*^{Int} intestine at E13.5, after forced BARX1 expression but before development of muscle hypertrophy. We cultured cells for 3 days to deplete endoderm (Kim et al., 2005) and used microarrays to evaluate mRNA expression in highly enriched mesenchymal cells. Principal component analysis (Fig. 6A) and unsupervised hierarchical clustering (Fig. 6B) revealed that expression profiles in *Barx1*^{Int} intestinal mesenchyme resembled wild-type stomach about as much as they did wild-type intestinal mesenchyme. Importantly, fewer than 200 genes showed significantly different levels in wild-type embryonic stomach and intestinal mesenchyme (Suppl. Table 1) and many transcripts that changed in *Barx1*^{Int} intestinal mesenchyme (Suppl. Table 2) corresponded to these differentially expressed genes (Fig. 6C). Nearly 2/3 of genes activated in *Barx1*^{Int} mesenchyme are selectively expressed in wild-type stomach mesenchyme and 2/3 of

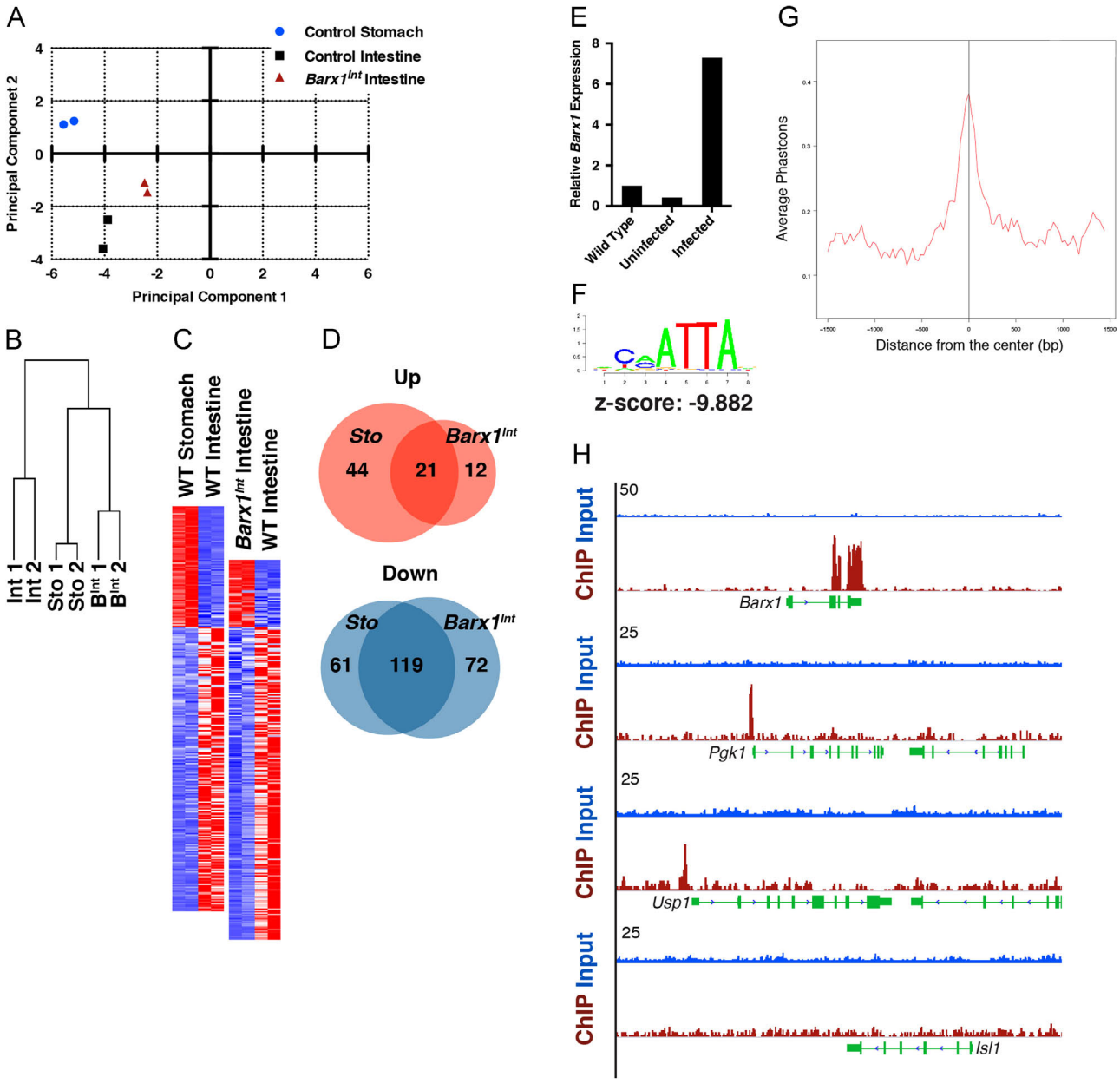

Fig. 6. Transcriptional control of stomach mesenchyme. (A and B) Principal component analysis (A) and unsupervised hierarchical clustering (B) of gene expression profiles indicates reproducible data from replicate samples and similarities between cultured wild-type stomach and *Barx1*^{Int} mesenchyme. (C) Heatmaps of mRNAs altered $\geq$2-fold in wild-type (WT) stomachs (left) and *Barx1*^{Int} intestines (right), both compared to WT intestines. Red, elevated expression; blue, reduced expression. (D) Venn diagrams representing transcripts expressed at higher (red) and lower (blue) levels in control stomachs and *Barx1*^{Int} intestines compared to WT intestines. (E) qRT-PCR evidence for expression of Flag-tagged *Barx1* in immortalized embryonic stomach mesenchymal cells. (F) Significant enrichment of the BARX1 consensus motif at occupied sites. (G) Graph showing evolutionary conservation of BARX1 binding sites in 8 mammalian species. (H) Integrated Genome Viewer traces of input (blue) and BARX1 ChIP (crimson) fragment reads (tag counts are represented on the *y*-axis) at 3 significant binding sites (top 3 examples), including the *Barx1* gene, and in the *Isl1* locus (bottom example).

intestine-selective genes were reduced in *Barx1*^{Int} intestinal mesenchyme (Fig. 6D). These observations implicate BARX1 as a crucial determinant of stomach mesenchyme, accounting for much of the difference from its intestinal counterpart.

This expression analysis confirmed absence of changes in Hh-dependent or Hh-effector genes in *Barx1*^{Int} mesenchyme (data not shown) and few cardinal myogenic regulatory genes were dysregulated at E13.5, before notable muscle expansion. Moreover, we detected few overall transcriptional changes, even though ectopic BARX1 expression leads to substantive later defects and even though most TFs regulate hundreds of genes (Biggin, 2011). To consider the possibility that BARX1 controls few genes directly, and myogenesis or other developmental functions indirectly, we used chromatin immunoprecipitation (ChIP) to map its cistrome. As available BARX1 Ab perform poorly in ChIP, we expressed FLAG epitope-tagged BARX1 in immortalized E13.5 mouse embryonic stomach mesenchymal cells (Fig. 6E) and used FLAG Ab for ChIP. In agreement with the few transcripts affected by BARX1 *in vivo*, we identified only 294 sites of BARX1 occupancy (false discovery rate, $q < 0.1$), which contrasted sharply with the ~10,000 binding sites we had identified separately for FLAG-tagged ATOH1 in adult intestinal crypt cells (Kim et al., 2014). These 294 sites showed phylogenetic conservation, indicating *bona fide* cis-regulatory elements, and the BARX1 consensus sequence was the most highly enriched motif, which implies direct TF binding (Fig. 6F and G). Moreover, we detected strong binding at the *Barx1* locus –

A

	Barx1^{Int} Intestine			Control Stomach		
	Fold Change vs. WT Intestine	SD	P Value	Fold Change vs. WT Intestine	SD	P Value
Isl1	23.43	0.37	***	19.79	1.23	**
Barx1	12.92	0.85	**	27.31	0.41	***
Isl1	7.50	0.26	**	6.60	0.28	**
Pitx1	5.04	0.08	**	8.62	0.77	*
Six2	4.65	0.19	**	4.25	0.37	*
HoxA9	3.73	0.40	*	3.06	0.03	*
Pitx2	3.54	0.01	***	3.33	0.29	*
Nr2f1	2.35	0.06	*	9.25	0.76	**
Prrx1	2.14	0.22	*	13.31	0.91	**

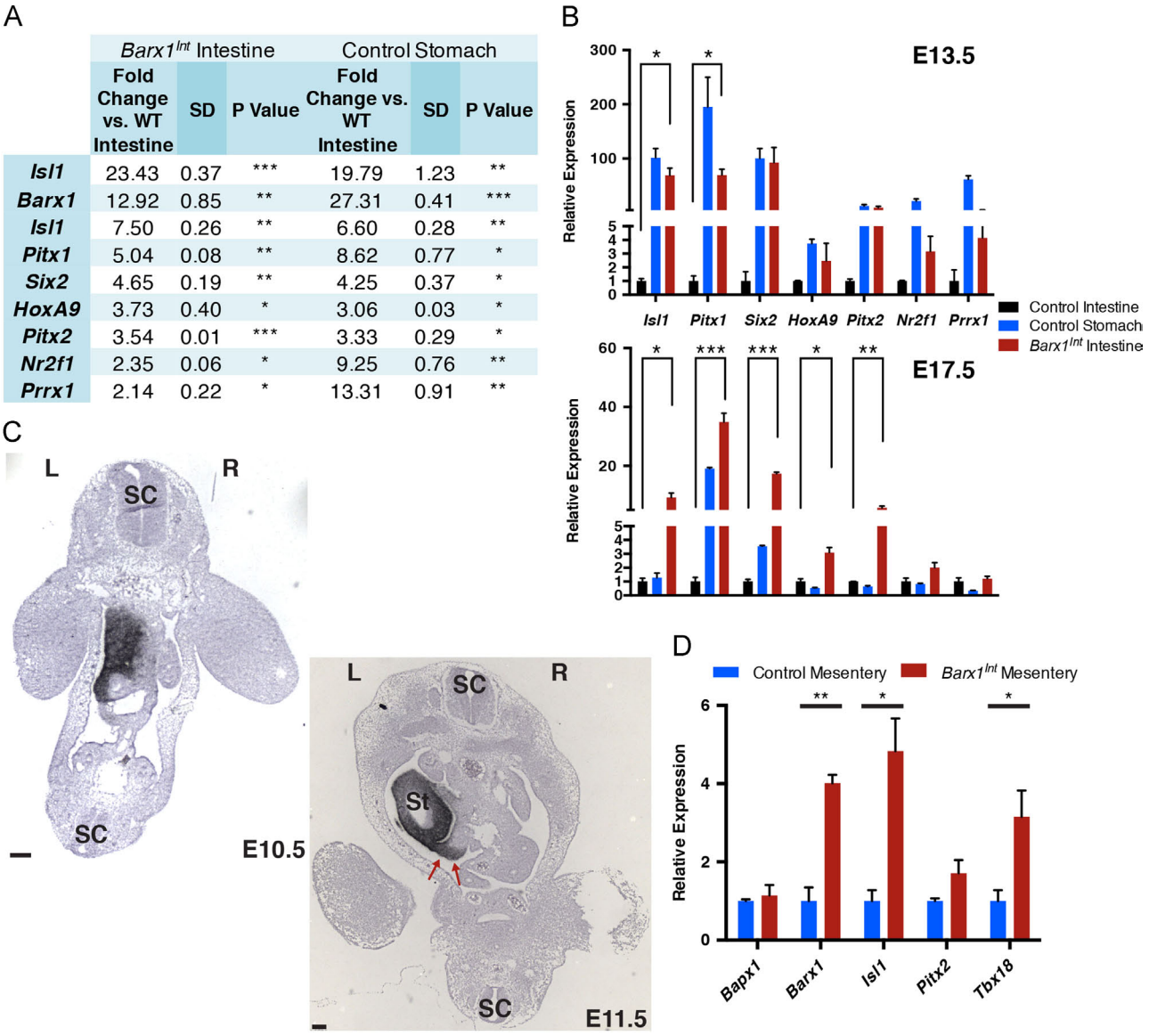

Fig. 7. *Barx1*-dependent transcription factor (TF) genes in the stomach mesenchyme and left abdominal mesentery. (A) Fold-changes, with standard deviations (SD) and *P*-values, for TF genes increased in E13.5 control stomachs and *Barx1*^{Int} intestines, compared to wild-type intestines. $^{*}P<0.05$, $^{**}P<0.005$, $^{***}P<.0005$. (B) qRT-PCR analysis of BARX1-dependent TF genes in mesenchyme purified from E13.5 (top, $n=2$ for each genotype and tissue) and E17.5 (bottom, $n=3$ each) wild-type (control) stomachs, intestines, and *Barx1*^{Int} intestines. The bars represent mean ± SEM of replicate samples. $^{*}P<0.05$, $^{**}P<0.005$, $^{***}P<.0005$. The TF mRNAs track with *Barx1* in E13.5 and E17.5 wild-type stomach mesenchyme and their levels are sustained in E17.5 *Barx1*^{Int} intestines. (C) *Barx1* mRNA in situ hybridization on coronal sections from E10.5 (top left) wild-type mouse embryos, revealing markedly asymmetric expression in early mesentery-abundant on the left (L) and absent on the right (R), with persistent L–R asymmetry in the E11.5 (bottom right) wild-type mesentery, contiguous with the stomach (St) anlage. SC, spinal cord. Scale bars, 200 μm. (D) qRT-PCR analysis of TF genes implicated in L–R visceral asymmetry in isolated E17.5 *Barx1*^{Int} and littermate control mesenteries.

suggesting autoregulation, a common feature of developmental TFs (Davidson, 2006) – and near several other genes (e.g., *Pgk1* and *Usp1* promoters, Fig. 6H). As most BARX1 binding occurs far from gene bodies, it is difficult to assign binding sites confidently to specific genes (Suppl. Table 3 lists all genes located within 100 kb of BARX1 binding), but very few genes with altered RNA expression in *Barx1*^{Int} mesenchyme showed nearby binding. Together, these observations suggest that BARX1 may execute many of its functions indirectly, acting through intermediary factors.

Indeed, the largest category of differentially expressed genes in *Barx1*^{Int} intestines, and the one with expression changes of the highest magnitude, encodes TFs with known roles in development (Fig. 7A, Suppl. Table 1); such TFs are ideal candidates for an intermediary role. *Six2* in particular has important functions in myogenesis, acting upstream of *Myod* (Relaix et al., 2013a), with a well-defined requirement in forming distal stomach muscle (Self et al., 2009) and Pitx2 controls extra-ocular myogenesis (Zacharias et al., 2011a). *Isl1* and *Pitx2* are further implicated in abdominal laterality; both TFs are restricted to the left side and a complementary factor, *Tbx18*, is confined to the right side (Davis et al., 2008; Kurpios et al., 2008; Logan et al., 1998; Ryan et al., 1998). qRT-PCR analysis of fresh isolates of E13.5 mesenchymal cells revealed 10- to >100-fold higher levels of each TF mRNA in wild-type stomach, relative to the intestine, and comparable elevations in *Barx1*^{Int} intestinal mesenchyme (Fig. 7B). In purified E17.5 stomach mesenchymal cells, many TF genes returned to the low levels found in the intestine, whereas *Pitx1* and *Six2* mRNAs remained high (3.5- to 20-fold), though far less than in E13.5 stomach (≥100-fold). However, all these TF mRNAs remained elevated in E17.5 *Barx1*^{Int} intestinal mesenchyme, in parallel with *Barx1* (Fig. 7B). Thus, BARX1 may act primarily by controlling TF genes, such as *Isl1*, *Pitx1*, *Pitx2* and *Six2*.

As asymmetries in the abdominal mesentery underlie fetal intestinal rotation (Davis et al., 2008; Kurpios et al., 2008) and the visceral looping defect in *Barx1*^{Int} embryos closely resembles that reported in mice with enforced symmetry of *Pitx2* expression (Shiratori et al., 2006), we asked next if these putative secondary TFs might plausibly mediate the completely penetrant gut malrotation seen in *Barx1*^{Int} embryos. The domain of *Barx1* mRNA in wild-type E10.5 (Fig. 7C top left) and E11.5 (Fig. 7C bottom right) mesentery is markedly asymmetric: expression is confined to the left side, contiguous with the splanchnic mesenchyme and extending toward the proximal intestine on the left side (red arrows in Fig. 7C bottom right), but not to distal loops on the right. This domain overlaps both with that of *Isl1* and *Pitx2* mRNAs (Davis et al., 2008; Kurpios et al., 2008) and with the site of invariable fusion of the duodenum to the stomach wall in *Barx1*^{Int} embryos (Fig. 2D,F,G). Moreover, elevated *Barx1* mRNA in *Barx1*^{Int} mesentery, expected because *Bapx1-Cre* is expressed in the mesentery, was associated with elevated levels of *Pitx2* and especially *Isl1* mRNAs (Fig. 7D). Moreover, elevated levels of *Tbx18* in isolated whole mesentery (Fig. 7D) indicated disrupted left–right patterning. Together, these findings support a model in which BARX1 controls expression of other tissue-restricted TF genes in the stomach mesenchyme and in mesentery on the left side.

4. Discussion

This study extends understanding of the roles and mechanisms of a pivotal developmental regulator, *Barx1*, beyond its previously established function in specifying the stomach epithelium and expanding the spleen. By investigating the results of forced *Barx1* expression in the *Bapx1* domain, together with reanalysis of *Barx1*$^{-/-}$ embryos, we uncovered additional activities in stomach myogenesis and intestinal rotation. Thick, well-developed smooth muscle is a cardinal feature of the stomach, distinct from the delicate intestinal musculature, and is necessary for the mechanical breakdown of solid foods. *Barx1*^{Int} intestines showed histologic features of stomach muscle and increased proliferation of muscle progenitors, whereas *Barx1*$^{-/-}$ stomachs showed reduced proliferation and numbers of smooth muscle cells. Thus, *Barx1* promotes stomach muscle at the expense of other mesenchymal cells, an activity that seems to account for the principal differences between gastric and intestinal muscle. Although *Barx1* loss induced epithelium of an intestinal type in the stomach (Kim et al., 2005), ectopic *Barx1* expression in intestinal mesenchyme did not perturb epithelial differentiation significantly, with discernible defects limited to a subtle widening of intestinal villi (Fig. 3). An important role for enteric smooth muscle was recently proposed in villus morphogenesis (Shyer et al., 2013) and the villus defect in *Barx1*^{Int} intestines may well represent a consequence of excess underlying muscle. Additionally, ectopic BARX1 expression invariably resulted in significant shortening of the intestine, for unclear reasons. We conclude that stomach mucosal features are not an inevitable consequence of *Barx1* expression in the underlying mesenchyme, but reflect the outcome of specific tissue interactions in the anterior foregut. In wild-type mid-gestation embryos, *Barx1* is transiently expressed at high levels in stomach mesenchymal cells and the mesentery, but is excluded from endoderm; its effects on epithelial differentiation are therefore indirect. By contrast, the effects on myogenesis occur in Barx1+ mesenchymal cells, revealing cell-autonomous activity in gastric smooth muscle development.

In addition to foregut mesenchyme, *Barx1* is expressed transiently in the left mesentery, contiguous with splanchnic mesenchyme, and our study revealed unexpected consequences of sustained, likely symmetric *Barx1* activity in this abdominal structure. Highly penetrant anomalies in *Barx1*^{Int} embryos included gastroschisis, intestinal and pancreatic hypoplasia, and asplenia (Fig. 2); in contrast, *Barx1*$^{-/-}$ embryos have a hypoplastic spleen containing the correct cell complement (Kim et al., 2007). As recent work reveals an instructive role for Wnt signaling and *Pitx2* in development of abdominal wall muscles and closure of the ventral body wall (Zhang et al., 2014), prominent gastroschisis in *Barx1*^{Int} embryos (Fig. 2B and C) could be a direct consequence of Barx1's known inhibition of Wnt signaling in other abdominal tissues (Kim et al., 2005; 2007; Woo et al., 2011). Alternatively, gastrochisis may be an indirect consequence of gut malrotation. Because intestinal rotation is known to depend on asymmetries in the dorsal mesentery (Davis et al., 2008; Kurpios et al., 2008), where ectopic BARX1 disturbs expression of key TF genes (Fig. 7), we attribute the gut malrotation and associated gastro-duodenal fusion in *Barx1*^{Int} mice to gene dysregulation in the early dorsal mesentery.

It is surprising, in this light, that an excess of BARX1 affected only a few dozen genes in gut mesenchymal cells. However, wild-type E13.5 stomach and intestinal mesenchyme also differed little in transcript profiles and ectopic *Barx1* was sufficient to drive much of the stomach-specific transcriptional program in intestinal mesenchyme. The most notable component of this program is a handful of TF genes, including *Pitx2*, *Isl1* and *Six2*, that can together account for the diverse developmental consequences. Expression of each of these putative target and effector genes parallels that of *Barx1* in wild-type, *Barx1*^{Int} and *Barx1*$^{-/-}$ mesenchyme and in *Barx1*^{Int} mesentery. Although we did not detect BARX1 occupancy within 50 kb of these TF genes, our experiments in cultured stomach mesenchymal cells may have captured only part of the full cistrome or BARX1 may activate them from a greater distance or indirectly. Nevertheless, these TFs are ideal candidate mediators of crucial *Barx1* activity because they are independently implicated in each of these functions. *Isl1*+ progenitor cells differentiate into smooth muscle in other tissues (Moretti et al., 2006). Levels of *Pitx1* and *Pitx2* rise during myogenesis and both TFs enhance myogenic differentiation in satellite cell-derived myoblasts (Knopp et al., 2013). Six-family proteins activate *MyoD* and control myogenesis (Relaix et al., 2013b), with a particular role for *Six2* in forming gastric pyloric muscle (Self et al., 2009). *Pitx2* and *Isl1* also determine L-R abdominal asymmetry and drive intestinal rotation (Davis et al., 2008; Kurpios et al., 2008), and the duodenal malrotation seen in *Barx1*^{Int} embryos is very similar to the defect that occurs when *Pitx2* expression is symmetric (Shiratori et al., 2006).

5. Conclusions

The sum of defects in *Barx1*^{Int} and *Barx1*$^{-/-}$ embryo reveals this homeodomain TF's potent role in patterning the abdominal organs. Our findings suggest that diverse BARX1 functions in different cells occur through a core group of intermediary TFs. In wild-type mesentery, BARX1-regulated asymmetric expression of *Pitx2* and *Isl1* enables proper intestinal rotation. BARX1 activates the same secondary TFs, and others such as *Six2*, in the stomach mesenchyme, leading to the characteristic differences between intestinal and gastric smooth muscle.

Acknowledgments

Supported in part by National Institutes of Heath Grant R01DK081113. We thank Byeong-Moo Kim, Janghee Woo and Justina Chen for crucial efforts in early phases of the work; Isabelle Miletich and Paul Sharpe for *Barx1* knockout mice and in situ

hybridization; Warren Zimmer for the gift of *Bapx1*^{Cre} mice; William Hahn for providing a p53DD plasmid; Christopher Wright for PDX1 antiserum; and Unmesh Jadhav, Kazu Murata, Maddie Saxena and Adrianna San Roman for helping complete experiments during manuscript revision.

Appendix A. Supplementary Information

Supplementary data associated with this article can be found in the online version at http://dx.doi.org/10.1016/j.ydbio.2015.05.024.

References

Biggin, M.D., 2011. Animal transcription networks as highly connected, quantitative continua. Dev. Cell 21, 611–626.
Davidson, E.H., 2006. The regulatory genome. Gene regulatory Networks in Development and Evolution. San Diego: Academic Press.
Davis, N.M., Kurpios, N.A., Sun, X., Gros, J., Martin, J.F., Tabin, C.J., 2008. The chirality of gut rotation derives from left-right asymmetric changes in the architecture of the dorsal mesentery. Dev. Cell *15*, 134–145.
Kim, B.M., Buchner, G., Miletich, I., Sharpe, P.T., Shivdasani, R.A., 2005. The stomach mesenchymal transcription factor Barx1 specifies gastric epithelial identity through inhibition of transient Wnt signaling. Dev. Cell 8, 611–622.
Kim, B.M., Miletich, I., Mao, J., McMahon, A.P., Sharpe, P.A., Shivdasani, R.A., 2007. Independent functions and mechanisms for homeobox gene Barx1 in patterning mouse stomach and spleen. Development 134, 3603–3613.
Kim, T.H., Li, F., Ferreiro-Neira, I., Ho, L.L., Luyten, A., Nalapareddy, K., Long, H., Verzi, M., Shivdasani, R.A., 2014. Broadly permissive intestinal chromatin underlies lateral inhibition and cell plasticity. Nature 506, 511–515.
Knopp, P., Figeac, N., Fortier, M., Moyle, L., Zammit, P.S., 2013. Pitx genes are redeployed in adult myogenesis where they can act to promote myogenic differentiation in muscle satellite cells. Dev. Biol. 377, 293–304.
Kosinski, C., Stange, D.E., Xu, C., Chan, A.S., Ho, C., Yuen, S.T., Mifflin, R.C., Powell, D. W., Clevers, H., Leung, S.Y., et al., 2010. Indian hedgehog regulates intestinal stem cell fate through epithelial-mesenchymal interactions during development. Gastroenterology 139, 893–903.
Kurpios, N.A., Ibanes, M., Davis, N.M., Lui, W., Katz, T., Martin, J.F., Izpisua Belmonte, J.C., Tabin, C.J., 2008. The direction of gut looping is established by changes in the extracellular matrix and in cell:cell adhesion. Proc. Natl. Acad. Sci. USA 105, 8499–8506.
Livak, K.J., Schmittgen, T.D., 2001. Analysis of relative gene expression data using real-time quantitative PCR and the 2(-Delta Delta C(T)) method. Methods 25, 402–408.
Logan, M., Pagan-Westphal, S.M., Smith, D.M., Paganessi, L., Tabin, C.J., 1998. The transcription factor Pitx2 mediates situs-specific morphogenesis in response to left-right asymmetric signals. Cell 94, 307–317.
Mao, J., Kim, B.M., Rajurkar, M., Shivdasani, R.A., McMahon, A.P., 2010. Hedgehog signaling controls mesenchymal growth in the developing mammalian digestive tract. Development 137, 1721–1729.
Moretti, A., Caron, L., Nakano, A., Lam, J.T., Bernshausen, A., Chen, Y., Qyang, Y., Bu, L., Sasaki, M., Martin-Puig, S., et al., 2006. Multipotent embryonic Isl1+ progenitor cells lead to cardiac, smooth muscle, and endothelial cell diversification. Cell 127, 1151–1165.
Powell, D.W., Pinchuk, I.V., Saada, J.I., Chen, X., Mifflin, R.C., 2011. Mesenchymal cells of the intestinal lamina propria. Annu. Rev. Physiol. 73, 213–237.
Ramalho-Santos, M., Melton, D.A., McMahon, A.P., 2000. Hedgehog signals regulate multiple aspects of gastrointestinal development. Development 127, 2763–2772.
Relaix, F., Demignon, J., Laclef, C., Pujol, J., Santolini, M., Niro, C., Lagha, M., Rocancourt, D., Buckingham, M., Maire, P., 2013a. Six homeoproteins directly activate Myod expression in the gene regulatory networks that control early myogenesis. PLoS Genet. 9, e1003425.
Relaix, F., Demignon, J., Laclef, C., Pujol, J., Santolini, M., Niro, C., Lagha, M., Rocancourt, D., Buckingham, M., Maire, P., 2013b. Six homeoproteins directly activate Myod expression in the gene regulatory networks that control early myogenesis. PLoS Genet. 9, e1003425.
Ryan, A.K., Blumberg, B., Rodriguez-Esteban, C., Yonei-Tamura, S., Tamura, K., Tsukui, T., de la Pena, J., Sabbagh, W., Greenwald, J., Choe, S., et al., 1998. Pitx2 determines left-right asymmetry of internal organs in vertebrates. Nature 394, 545–551.
Savin, T., Kurpios, N.A., Shyer, A.E., Florescu, P., Liang, H., Mahadevan, L., Tabin, C.J., 2011. On the growth and form of the gut. Nature 476, 57–62.
Self, M., Geng, X., Oliver, G., 2009. Six2 activity is required for the formation of the mammalian pyloric sphincter. Dev. Biol. 334, 409–417.
Shaulian, E., Zauberman, A., Ginsberg, D., Oren, M., 1992. Identification of a minimal transforming domain of p53: negative dominance through abrogation of sequence-specific DNA binding. Mol. Cell. Biol. 12, 5581–5592.
Shiratori, H., Yashiro, K., Shen, M.M., Hamada, H., 2006. Conserved regulation and role of Pitx2 in situs-specific morphogenesis of visceral organs. Development 133, 3015–3025.
Shyer, A.E., Tallinen, T., Nerurkar, N.L., Wei, Z., Gil, E.S., Kaplan, D.L., Tabin, C.J., Mahadevan, L., 2013. Villification: how the gut gets its villi. Science 342, 212–218.
Spence, J.R., Lauf, R., Shroyer, N.F., 2011. Vertebrate intestinal endoderm development. Dev. Dyn. 240, 501–520.
Srinivas, S., Watanabe, T., Lin, C.S., William, C.M., Tanabe, Y., Jessell, T.M., Costantini, F., 2001. Cre reporter strains produced by targeted insertion of EYFP and ECFP into the ROSA26 locus. BMC Dev. Biol. 1, 4.
Sukegawa, A., Narita, T., Kameda, T., Saitoh, K., Nohno, T., Iba, H., Yasugi, S., Fukuda, K., 2000. The concentric structure of the developing gut is regulated by Sonic hedgehog derived from endodermal epithelium. Development 127, 1971–1980.
Verzi, M.P., Shin, H., He, H.H., Sulahian, R., Meyer, C.A., Montgomery, R.K., Fleet, J.C., Brown, M., Liu, X.S., Shivdasani, R.A., 2010. Differentiation-specific histone modifications reveal dynamic chromatin interactions and partners for the intestinal transcription factor CDX2. Dev. Cell 19, 713–726.
Verzi, M.P., Stanfel, M.N., Moses, K.A., Kim, B.M., Zhang, Y., Schwartz, R.J., Shivdasani, R.A., Zimmer, W.E., 2009. Role of the homeodomain transcription factor Bapx1 in mouse distal stomach development. Gastroenterology 136, 1701–1710.
Woo, J., Miletich, I., Kim, B.M., Sharpe, P.T., Shivdasani, R.A., 2011. Barx1-mediated inhibition of Wnt signaling in the mouse thoracic foregut controls tracheoesophageal septation and epithelial differentiation. PLoS One 6, e22493.
Zacharias, A.L., Lewandoski, M., Rudnicki, M.A., Gage, P.J., 2011a. Pitx2 is an upstream activator of extraocular myogenesis and survival. Dev. Biol. 349, 395–405.
Zacharias, W.J., Madison, B.B., Kretovich, K.E., Walton, K.D., Richards, N., Udager, A. M., Li, X., Gumucio, D.L., 2011b. Hedgehog signaling controls homeostasis of adult intestinal smooth muscle. Dev. Biol. 355, 152–162.
Zambrowicz, B.P., Imamoto, A., Fiering, S., Herzenberg, L.A., Kerr, W.G., Soriano, P., 1997. Disruption of overlapping transcripts in the ROSA beta geo 26 gene trap strain leads to widespread expression of beta-galactosidase in mouse embryos and hematopoietic cells. Proc. Natl. Acad. Sci. USA 94, 3789–3794.
Zhang, J., Rosenthal, A., de Sauvage, F.J., Shivdasani, R.A., 2000. Downregulation of hedgehog signaling is required for organogenesis of the small intestine in Xenopus. Dev. Biol. 229, 188–202.
Zhang, L., Li, H., Yu, J., Cao, J., Chen, H., Zhao, H., Zhao, J., Yao, Y., Cheng, H., Wang, L., et al., 2014. Ectodermal Wnt signaling regulates abdominal myogenesis during ventral body wall development. Dev. Biol. 387, 64–72.